Robert Konecny[1–3]
Joanna Trylska[1,2,4]
Florence Tama[2,5]
Deqiang Zhang[1,2,7]
Nathan A. Baker[6]
Charles L. Brooks, III[2,5]
J. A. McCammon[1,2,7]

[1] *Department of Chemistry and Biochemistry, University of California at San Diego, 9500 Gilman Drive, La Jolla, CA 92093-0365*

[2] *Center for Theoretical Biological Physics, University of California at San Diego, 9500 Gilman Drive, La Jolla, CA 92093-0374*

[3] *W. M. Keck Laboratory for Integrated Biology II, University of California at San Diego, 9500 Gilman Drive, La Jolla, CA 92093-0365*

[4] *ICM Warsaw University, Pawinskiego 5a, 02-106 Warsaw, Poland*

Electrostatic Properties of Cowpea Chlorotic Mottle Virus and Cucumber Mosaic Virus Capsids

[5] *Department of Molecular Biology, Scripps Research Institute, 10550 North Torrey Pines Road, La Jolla, CA 92037*

[6] *Department of Biochemistry & Molecular Biophysics and Center for Computational Biology, Washington University School of Medicine, St. Louis, MO 63110*

[7] *Howard Hughes Medical Institute and Department of Pharmacology, University of California at San Diego, La Jolla, CA 92093-0365*

Received 18 August 2005; revised 28 October 2005; accepted 31 October 2005
Published online 8 November 2005 in Wiley InterScience (www.interscience.wiley.com).
DOI 10.1002/bip.20409

Abstract: *Electrostatic properties of cowpea chlorotic mottle virus (CCMV) and cucumber mosaic virus (CMV) were investigated using numerical solutions to the Poisson–Boltzmann equation. Experimentally, it has been shown that CCMV particles swell in the absence of divalent cations when the pH is raised from 5 to 7. CMV, although structurally homologous, does not undergo this transition. An analysis of the calculated electrostatic potential confirms that a strong electrostatic repulsion at the calcium-binding sites in the CCMV capsid is most likely the driving force for the capsid swelling process during the release of calcium. The binding interaction between the encapsulated genome material (RNA) inside of the capsid*

Correspondence to: Robert Konecny; e-mail: rok@ucsd.edu
Contract grant sponsor: NIH, NSF, the National Biomedical Computing Resource, CTBP, and Accelrys, Inc.
Biopolymers, Vol. 82, 106–120 (2006)

and the inner capsid shell is weakened during the swelling transition. This probably aids in the RNA release process, but it is unlikely that the RNA is released through capsid openings due to unfavorable electrostatic interaction between the RNA and capsid inner shell residues at these openings. Calculations of the calcium binding energies show that Ca^{2+} can bind both to the native and swollen forms of the CCMV virion. Favorable binding to the swollen form suggests that Ca^{2+} ions can induce the capsid contraction and stabilize the native form. Biopolymers 82: 106–120, 2006

This article was originally published online as an accepted preprint. The ''Published Online'' date corresponds to the preprint version. You can request a copy of the preprint by emailing the Biopolymers editorial office at biopolymers@wiley.com

Keywords: *computational modeling; supramolecular assembly; Poisson–Boltzmann equation; electrostatic potential; simulation; normal mode analysis; swelling; electrostatic binding energy*

INTRODUCTION

Assembly and disassembly of a viral capsid, or a protein shell, are essential steps in the life cycle of a virus. Understanding of viral assembly/disassembly can provide additional insights to other oligomerization processes as in protein association in large cellular assemblies, which occurs through a similar mechanism. Additionally, understanding the properties and function of the capsid shell alone is important for inferring all steps involved in host cell entry and release of the enveloped genetic material and can aid in proposing efficient ways of interfering with capsid assembly and stability via structure-based design of antiviral therapeutics.

One of the most intensely studied viruses has been the cowpea chlorotic mottle virus (CCMV), a positive-strand RNA plant-infecting virus that belongs to the Bromoviridae family (Figure 1a and b). It is composed of a protein capsid and viral RNA that is packed inside. It has been widely used as a model system for understanding of biological assembly because of its icosahedral structure and the limited number of gene products required for its assembly. CCMV offers an accessible model system for examining the processes that regulate viral assembly, disassembly, and stability, both for theoretical and experimental studies.

The crystal structure of CCMV has been solved to 3.2 Å resolution.[1] The CCMV virion is comprised of 180 copies of the coat protein subunits arranged with $T = 3$ quasi-symmetry and organized in 20 hexameric and 12 pentameric capsomers (Figure 2). Each coat protein subunit consists of a β-barrel fold (residues 52–176) from which long N-terminal (residues 1–51) and C-terminal arms (residues 176–190) extend in opposite directions (Figure 2a). The individual pentameric and hexameric capsomers are linked into a comprehensive network by the coat protein C-termini. Additionally, each extended C-terminus is anchored by being clamped between the β-barrel core and the N-proximal loop of its partner subunit. The N-terminal arm of the coat protein participates in three different types of interactions. The first 26 amino acids are very basic and interact with negatively charged viral RNA. Amino acids 27–35 form the β-hexamer, which stabilizes hexameric capsomers, and amino acids 44–51 form the clamp for the extended C-terminal arm. This β-hexamer is located at the icosahedral threefold axes and is a variant of the β-annulus observed in many plant virus capsids.[2]

Inside the capsid, the single-stranded viral RNA is arranged as an interior shell, leaving the virion center hollow, and adopts an ordered conformation at each of the quasi-threefold axis. The N-terminal 26 amino acids of the coat protein, which are highly basic and required for RNA packaging,[3] extend into the interior of the capsid and interact with the RNA to neutralize phosphate charges. Additionally, the RNA interacts with 13 of the amino acids on the interior capsid surface. These include ionic interactions with number of lysines and arginines, and a stacking interaction between the base of two consecutive RNA nucleotides and a tryptophan side chain.

The capsid protein is multifunctional; in addition to having a role in encapsulation, it affects the viral movement in plants, transmission, symptom expression, and host range.

Native CCMV is stable at pH 5.0 but at pH 7.0 and in the absence of Ca^{2+} or Mg^{2+} the capsid diameter swells by approximately 10%. In this process the ionic strength remains low, $<0.2M$.[4,5] This swelling can also be induced just by increasing pH of the solution while ionic strength is kept constant.[1,6] Swelling

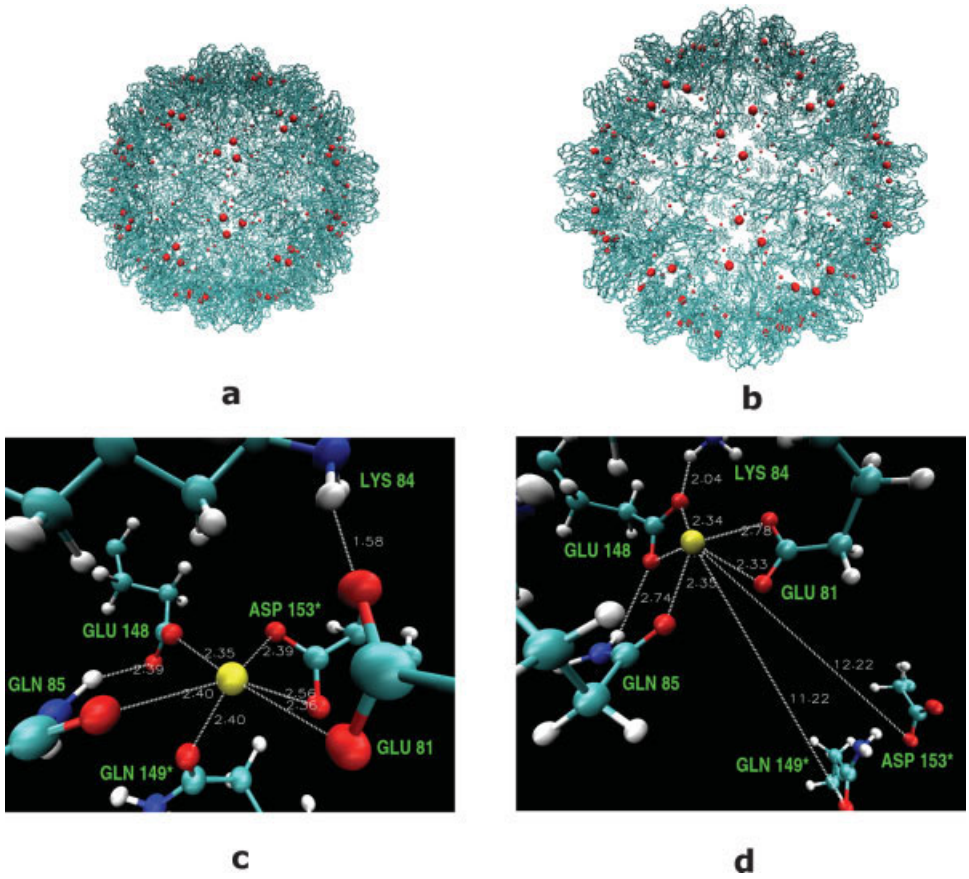

FIGURE 1 Backbone model of the CCMV capsid in the native (a) and swollen (b) state with calcium ions shown in red. Modeled calcium cavity residues in the native (c) and swollen (d) form of the CCMV virus. The most important distances from calcium ions (yellow spheres) are shown (in Å).

is the result of an expansion of the virion capsid at the pseudo-threefold axis while the contacts within the hexameric and pentameric morphological units are conserved (Figure 1a and b).[1] Although the swelling creates large openings in the capsid at the pseudo-threefold axis, the viral RNA is not spontaneously released, rendering the swelling reversible.[7,8] The capsid dimer subunit interactions are retained, but shifted in their geometry.[9,10] The expanded state is stabilized by dimer and β-hexamer intersubunit contacts and, predominantly, by RNA protein interactions. Empty capsids cannot swell without dissociating due to the absence of RNA–capsid stabilizing interaction. The biological significance of the swelling phenomenon is not well understood but it is believed this mechanism is related to RNA release during infection.

The assembly process is thought to be initiated by the association of two protein subunits forming dimers and, consequently, pentamer of dimers.[11] These form, with addition of other dimers, pentameric and

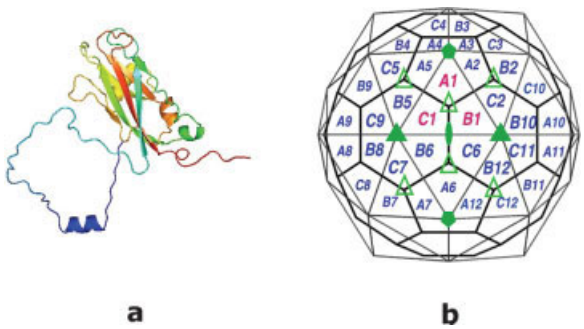

FIGURE 2 (a) A single CCMV capsid protein subunit (N-terminus arm blue, C-terminus is red). (b) Schematic representation of quasi-equivalent lattice model for CCMV. The 2-fold, 3-fold, and 5-fold axes are identified by filled oval, triangles, and pentagons, respectively. The pseudo-threefold axes are identified by empty triangles. The central triangle (labeled A1, B1, and C1) defines the icosahedral asymmetric unit. The polygons represent chemically identical protein subunits, which represent the three slightly different geometrical environments of the coat protein.[54]

hexameric capsomers. The overall assembly rate is high; infectious particles assemble in vitro in seconds.[3]

The first eight N-terminal amino acid residues are not essential for viral assembly in vitro; both empty and RNA-containing particles are assembled even when these residues are deleted.[3] However, deletion of the first 25 N-terminal residues eliminates the ability of the virus to assemble RNA-containing particles, although empty particles are still produced in vitro. This experimental result is also supported by our recent simulation study.[12] The deletion of the complete N-terminal arm prevents assembly of either RNA-containing or empty particles, presumably due to the importance of the β-hexamer structure for CCMV assembly.[3]

Based on several experimental mutation studies[4–6] Albert et al. proposed that swelling may not be required for the RNA release from the capsid, and that the pentameric capsomer can undergo a different structural transition by forming a channel through which the viral RNA passes and becomes available to the cell's replicating machinery.[6] This has been supported by a recent computational study of RNA diffusion through a pseudo-threefold channel in the capsid shell.[13] However, an alternative interpretation of the experimental observation has been put forward suggesting that a fraction of the virions swell at neutral pH.[14] The calcium electron density is not observed in the X-ray structure of the virus, but based on the experimental conditions of crystal growth and theoretical modeling, the calcium positions have been indicated.[1,9] Three binding sites for the calcium ions in one unit of the CCMV virus have been proposed. They are situated at the interfaces of the subunits A–B, B–C, and C–A (Figure 2b). The calcium cavity is composed mainly of glutamic and aspartic acids (Figure 1c and d). These acidic residues interacting with calcium have also been seen in other calcium binding systems, e.g., in EF-hand proteins.[15] Such a negatively charged surrounding is likely to bind a positively charged ion. It was proposed that binding of Ca^{2+} in the capsid cavities adds to the stability of the native virion.[1]

In a recent study,[16] the calcium ions have been shown to be essential for the viral stability and for the assembly of the capsid in another virus, simian virus 40. Experiments were performed in which the negatively charged residues in the calcium cavity were mutated into positively charged ones. The work has shown that the calcium ions mediate not only the virion assembly but also contribute to the initial process of cell entry. The studies were performed in vivo and provided the evidence for the controlled manner of calcium binding and release during the infection process. The study alsoconfirmed that the calcium affects the structural flexibility of the virion.

In this study we explore the electrostatic properties of the CCMV viral capsid and of cucumber mosaic virus (CMV) capsid. The CMV virus shows a remarkable similarity in overall architecture to CCMV but does not undergo the swelling phenomenon observed in CCMV.[2,9] While in CCMV, a cluster of acidic residues is found at the pseudo-threefold center, which is likely responsible for the swelling, no such clusters exist in CMV.[9,17] Analysis and comparison of electrostatic properties and in particular the electrostatic potential at the protei–protein interface at the pseudo-threefold centers between CCMV and CMV should offer insights into functional differences between these two viral capsids. We also investigated the energetics of calcium binding to CCMV capsid cavities. Because the process of swelling is believed to require the removal of Ca^{2+} and, on the other hand, is reversible, calcium has to show favorable binding to both of the forms: contracted and expanded. The relative electrostatic contribution to binding free energies of the site-bound Ca^{2+} ions to the native and swollen CCMV capsids were calculated in this study based on the solution of the Poisson–Boltzmann equation in continuum solvent.

MATERIALS AND METHODS

Theory

Poisson–Boltzmann Equation. The electrostatic calculations were based on Poisson–Boltzmann theory. For many years, this model has been successfully applied to biological molecules and the details of its implementation and application to such systems may be found in Refs. 18–20.

The differential Poisson equation describes the electrostatic potential $\Phi(\mathbf{r})$ in a medium with a dielectric scalar field $\varepsilon(\mathbf{r})$ and with a charge density $\rho(\mathbf{r})$

$$\nabla \cdot \varepsilon(\mathbf{r})\nabla\Phi(\mathbf{r}) = -4\pi\rho(\mathbf{r}) \quad (1)$$

In a solvated molecular system, the charge density is divided into the fixed interior charge distribution of the molecule, $\rho_{\text{int}}(\mathbf{r})$, and a mobile exterior charge density of the solvent and ions. The exterior is modeled as a dielectric continuum with the mobile ion density approximated by a Boltzmann distribution at temperature T. Equation (1), therefore, takes the form of a nonlinear Poisson–Boltzmann (PB) equation,

$$\nabla \cdot \varepsilon(\mathbf{r})\nabla\Phi(\mathbf{r}) = -4\pi\rho_{\text{int}}(\mathbf{r}) + \lambda(\mathbf{r})\bar{\kappa}^2 \sinh[\Phi(\mathbf{r})/kT] \quad (2)$$

where $\varepsilon(\mathbf{r})$ is the dielectric constant of the solute or the solvent, k is the Boltzmann constant, λ equals 1 for ion-acces-

sible regions and 0 elsewhere. The $\bar{\kappa}^2$ is the modified Debye–Hückel parameter defined as

$$\bar{\kappa}^2 = \frac{8\pi e^2 N_A I}{1000kT} \quad (3)$$

where N_A is the Avogadro constant, e the charge of an electron, and I the ionic strength. The nonlinear PB equation is often approximated by its linear form, which is easier to solve:

$$\nabla \cdot \varepsilon(\mathbf{r})\nabla\Phi(\mathbf{r}) = -4\pi\rho_{int}(\mathbf{r}) + \lambda(\mathbf{r})\bar{\kappa}^2\Phi(\mathbf{r}) \quad (4)$$

Normal Mode Analysis. Normal mode analysis (NMA) is a powerful technique to study large conformational rearrangements in biological systems. This approach generally entails the diagonalization of the matrix of second derivatives of the potential energy for the calculation of the independent collective modes of displacement. The direct calculation of atomic-level normal modes for viruses is computationally prohibitive for use in routine application, and some type of multiscale approach is necessary. One such approach, the elastic network model,[21] provides a simplified representation of the underlying energy surface for large systems that enables the study of the dynamics of these systems.[22,23] The elastic network models can be constructed and normal mode analysis can be performed based on Cα's, residue blocks, or even coarser granularities to yield good descriptions of large-scale conformational distortions in macromolecular assemblies.[24] Further computational efficiency can be gained without significant loss in information through the addition of the rotation-translation block (RTB) method for the diagonalization of the matrix of second derivatives.[25] In the present calculations we have used a Cα-only representation in constructing the elastic network models of the virus capsids and the RTB approach with individual blocks corresponding to each protein in the viral capsid for the normal mode calculations. Details of the elastic network models and associated normal mode methods can be found in the recent review by Tama and Brooks.[26]

It was established in our earlier studies of CCMV swelling that one of the lowest frequency normal modes well represents most of the conformational change observed between native and swollen CCMV.[9] Using the normal mode directions from these calculations, intermediate structures along the swelling pathway were proposed and examined to investigate the origins of the observed pH triggered swelling in CCMV, and the key role of calcium binding and pK_a shifts of acidic residues during expansion of the capsid were identified as critical components in the regulating the swelling process.[9] In the present work we have extended the analysis of the electrostatic properties associated with the swelling processes by combining the normal mode calculations with whole-capsid electrostatic calculations. Since the NMA was performed using only the Cα atoms, fully atomic structures were obtained by superimposing the atomic detailed structure onto the Cα framework and optimized in the presence of the symmetry-related neighbors.[9]

Ligand Binding Energy Calculations. The free energy of ligand–protein association may be approximated in the form[27,28]

$$\Delta G^{bind} = \Delta G_{elec} + \Delta G_{np} - T\Delta S \quad (5)$$

where ΔG_{elec} is the electrostatic contribution, ΔG_{np} the nonpolar or hydrophobic term, and $-T\Delta S$ describes the loss of entropy (conformational, translational, and rotational) upon complexation. The electrostatic term is often calculated using the continuum Poisson–Boltzmann model,[28,29] and the nonpolar term is estimated based on the amount of the solvent accessible surface area (SASA) buried upon binding. We apply the above equation to estimate the relative strength of binding of site-bound Ca^{2+} between the native and expanded forms of the viral capsid.

The electrostatic contribution to binding free energy may be written as[29]

$$\Delta G_{elec} = \Delta G_{elec}^{solv} + \Delta G_{elec}^{coul} \quad (6)$$

where the terms on the right are the electrostatic solvation (dehydration of ion upon binding) and coulombic pairwise charge–charge interaction, respectively. ΔG_{elec}^{solv} is the difference in energy of creating a dielectric boundary while immersing the complex, and the protein and calcium separately, in a high-dielectric medium. ΔG_{elec}^{coul} is the work of assembling the atomic charges in a dielectric medium characterizing the protein.

We would like to note that there have been attempts to treat divalent cation binding more accurately within the PBE theoretical framework than presented here,[30–32] but to rigorously account for ion desolvation and correlation as well as standard state issues divalent cations should be modeled explicitly. However, the present work only intends to focus on the changes in the electrostatic potential with viral capsid swelling, in a simple univalent ionic strength picture, and to note qualitatively the dramatic change in potential at the putative calcium binding site.

Computational Details

Electrostatic Calculations. The electrostatic calculations were performed using the Adaptive Poisson–Boltzmann Solver (APBS) package. The solution to the PBE is obtained as described by Baker et al.[33] Specifically, the problem domain is divided into overlapping subdomains thatare then used to assemble the final solution. The solution consists of a series of ''focusing'' calculations[29] from the global domain to the smaller overlapping subdomains. During this focusing algorithm, energy integrals are calculated over subsets of the domain that are (a) unique to the processor of interest and (b) not part of a finer level of calculation. By performing the energy calculations in this manner, we ensure that energy contributions from all regions of the domain are calculated without any contributions being double-counted.

Since the first 26 N-terminal amino acid residues of the coat protein are unresolved in the X-ray crystal structure, the CCMV native structure (PDB ID 1CWP)[1] with the

added and optimized network of missing residues (1–26) was taken from our previous study.[12] NMA was then used to generate the CCMV geometry of the swollen particle. The CMV geometry was obtained from the Protein Data Bank[34] (PDB ID 1F15).[2] However, in this case we did not add any residues that were missing from the X-ray crystal structure (residues 1–28). In all of the electrostatic calculations the Cα geometries were used except for those in which ligand-binding energies were computed, where the all-atom structures were employed. We performed several exploratory all-atom calculations, and the resulting electrostatic potential was very similar to the potential calculated with Cα-only models. A similar approach was used in our previous study.[35]

In all of the APBS calculations the solute and solvent were assigned a dielectric constant of 2 and 78.5, respectively. The ionic strength of monovalent ions was set to 0.150*M* with an ion exclusion radius of 2 Å. The dielectric boundary between solute and solvent was based on the molecular surface definition calculated with a probe sphere radius of 1.4 Å. For the boundary conditions, the focusing method was applied.[29,36] Similar protocol was used in our previous work.[12]

Considering the extremely large size of the system, the calculations were performed on the Blue Horizon and Data Star supercomputers using 1000 processors for each run. The dimensions of the CCMV capsid are $271 \times 271 \times 271$ Å^3 and $319 \times 319 \times 319$ Å^3 for the native and swollen forms (Cα model), respectively. The total charge of the system (modeled at pH 7) not including 180 calcium ions, with and without the missing 26 amino acid long N-terminal fragment,was $+900e$ and $-660e$, respectively. The PB equation was solved on $543 \times 543 \times 543$ Å^3 numerical grid (the same grid size and position was used for the native and swollen structures for consistency) to a resolution of 0.4 Å (more than 2.5 billion grid points) both for the linear and nonlinear forms of the PB equation. The CMV capsid was slightly larger compared to native CCMV ($285 \times 285 \times 285$ Å^3, Cα model), and the total charge is $+720e$. The CMV electrostatic calculation was performed on a $484 \times 484 \times 484$ Å^3 grid and the PB equation was solved to 0.4 Ã resolution (>1.7 billion grid points).

Ligand-Binding Calculations. The calcium electron density is not observed in the X-ray structure of the virus, but based on the experimental conditions of crystal growth and theoretical modeling, the calcium positions have been indicated.[1,9] For each structure, Ca^{2+} ions were added, with the position of calcium given by the average of the coordinates of the six ligands.[9] The hydrogens were added to each structure with CHARMM's HBUILD command,[37,38] according to the protonation states of the residues in solution at pH 7 (Asp, Glu, Lys, and Arg residues were assigned a net charge of -1 or $+1$, respectively; N- and C-termini were kept charged and all other residues had a net charge of 0), and their positions were energy-minimized to avoid bad contacts. The positions of the calcium ions were also optimized.

First, the APBS calculations were performed for each calcium cavity and one protein unit composed of three subunits A, B, and C. The calcium cavities are not exactly symmetric and the rearrangement of the residues in each cavity differs slightly. Therefore, we chose to perform calculations for each cavity A, B, and C and averaged the electrostatic contribution. For one protein unit three calciums were added at a time and the contribution was also averaged. We verified that adding one calcium separately to one protein unit and averaging over three ΔG_{elec} gives similar result (within 2 kcal/mol) if adding three calciums at a time to the unit and dividing the output electrostatic energy by three. The latter approach is less time-consuming; therefore it was used later.

Three force field models were applied: a united atom model (charmm19), an all-atom model (charmm22),[37,38] and a mixed charmm22/electrostatic potential (ESP) model. The latter included a combination of the ESP charges assigned to the calcium cavity atoms (details below) and the charmm22 parameters assigned to the rest of the protein. In case of calculations for the calcium cavity only, the third model included just the ESP charges.

To derive the ESP charges for the calcium cavity residues, quantum mechanical calculations using the Gaussian98[39] program were performed. The modeled system was composed of six protein residues and the calcium ion (see Figure 1c and d). The Cα-terminal atoms were modified into CH_3 groups. The configuration was taken exactly as in the energy-minimized protein. The density functional single point energy calculations with the B3LYP exchange and correlation functional[40,41] and 6–31 + G(d,p) basis set were carried out. The Breneman ESP-derived charges (ChelpG),[42] which gave a reduced partial charge on calcium of $+1.6e$, were used to calculate the APBS electrostatic energies with a mixed charmm22/ESP parameter model.

For the single calcium cavities, both the linear and nonlinear solutions of the PB equation converged up to a grid resolution of 0.15 Å; for the one protein unit the linear PBE converged up to 0.18 Å and nonlinear PBE to 0.35 Å; for the whole CCMV structure both PBE converged up to 0.4 Å. The overall charge of subunits A, B, and C including three Ca^{2+} ions is $-5e$; for one cavity it is $-2e$. The same grid positioning and spacing were applied, both for the complex and binding systems. The binding energies were calculated with two methods and compared. In the direct method we calculated the difference between the PB energies for the complex and its constituents, and in the additive method we calculated the differences in the solvation and coulombic contributions separately [see Eq. (6)]. The Coulomb interaction energy was evaluated as a pairwise charge–charge interaction.

The change in SASA was calculated with the acc utility of APBS.

RESULTS AND DISCUSSION

Cowpea Chlorotic Mottle Virus (CCMV)

The calculated electrostatic potential for the native and swollen CCMV particles is shown in Figure 3 (presented as isosurface at ± 1.0 kT/e). The outer

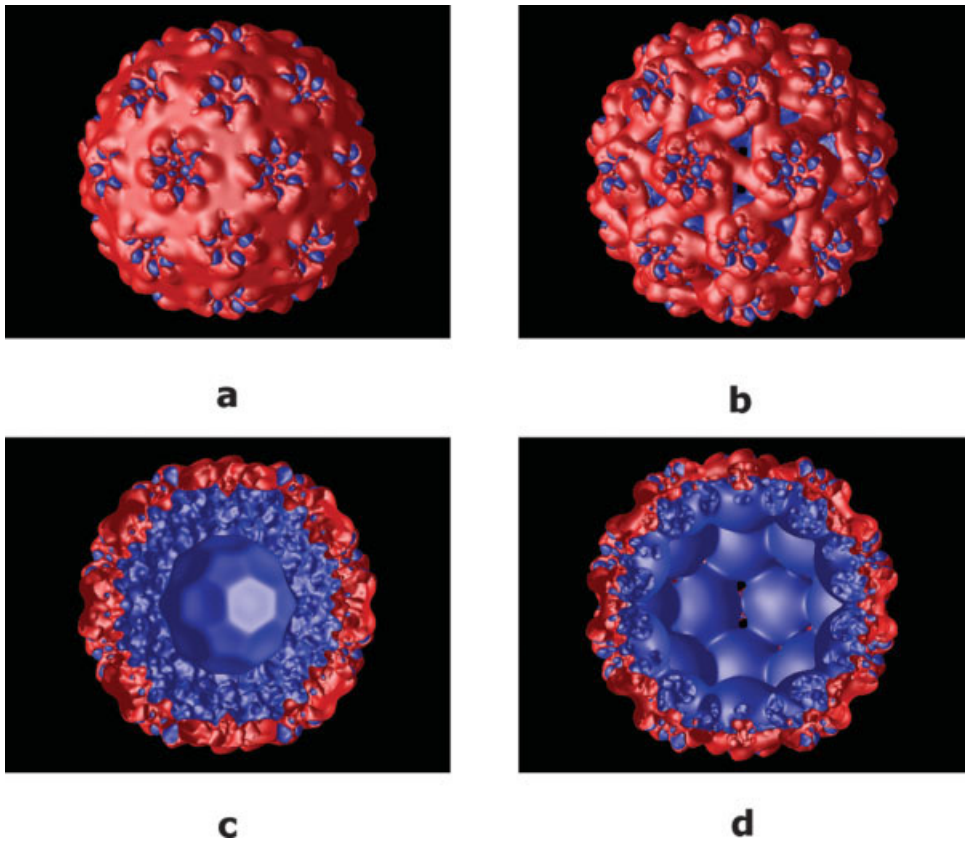

FIGURE 3 Calculated electrostatics isosurface (at $\pm 1.0\ kT/e$) of the native (a and c) and swollen (b and d) CCMV viral particle. Panels c and d show cut through the capsid. Blue and red colors represent positive and negative potential, respectively.

electrostatic potential surface (Figure 3a and b) is predominantly negative with patches of positive electrostatic potential concentrated at the top of the hexameric and pentameric subunits, retaining symmetrical elements of the capsid. The electrostatic potential of the inner capsid shell (Figure 3c and d) is mostly positive as expected, since the inner shell is formed primarily by basic amino acid residues. These residues facilitate binding to the negatively charged RNA.

Further insights can be gained when the calculated electrostatic potential is projected on the solvent accessible surface of the virion particle. This is shown in Figure 4 for both native and swollen structures. Again, the overall electrostatic potential at the outer capsid solvent accessible surface is negative (Figure 4a) and the highest concentration of the negative potential is at the pseudo-threefold axis sites. These sites are mainly composed of a cluster of negatively charged aspartic acid residues, which are proposed to bind metal ions in pH-dependent manner. It is very likely that when the metal ion is removed from this site (for example, by chelating to EDTA), the closely positioned negatively charged residues will experience strong electrostatic repulsion. One way for the capsid to relieve this strain is to increase interresidue distance at this site. This is exactly what happens when the capsid swells, as demonstrated by the earlier study of Tama and Brooks.[9] The largest geometrical change in terms of interatomic distances occurs at the pseudo-threefold axis sites. While the hexameric and pentameric subunits rotate in the plane of the capsid surface during the capsid expansion, the aspartic acid residues at the proposed metal binding site move laterally from each other, minimizing electrostatic repulsion (Figure 4c and d).

Positive electrostatic potential dominates at the inner CCMV surface shell, as seen in Figure 5. A major source of this positive potential is the basic residues located among the first 26 amino acid N-terminal residues. These residues are also responsible for the binding interaction with negatively charged RNA. Experimentally, it was shown that deletion of the first 26 N-terminal amino acid residues suppresses assembly of RNA-containing particles, but not empty particles in vitro.[3] We have calculated the electrostatic potential for the capsid without the first 26

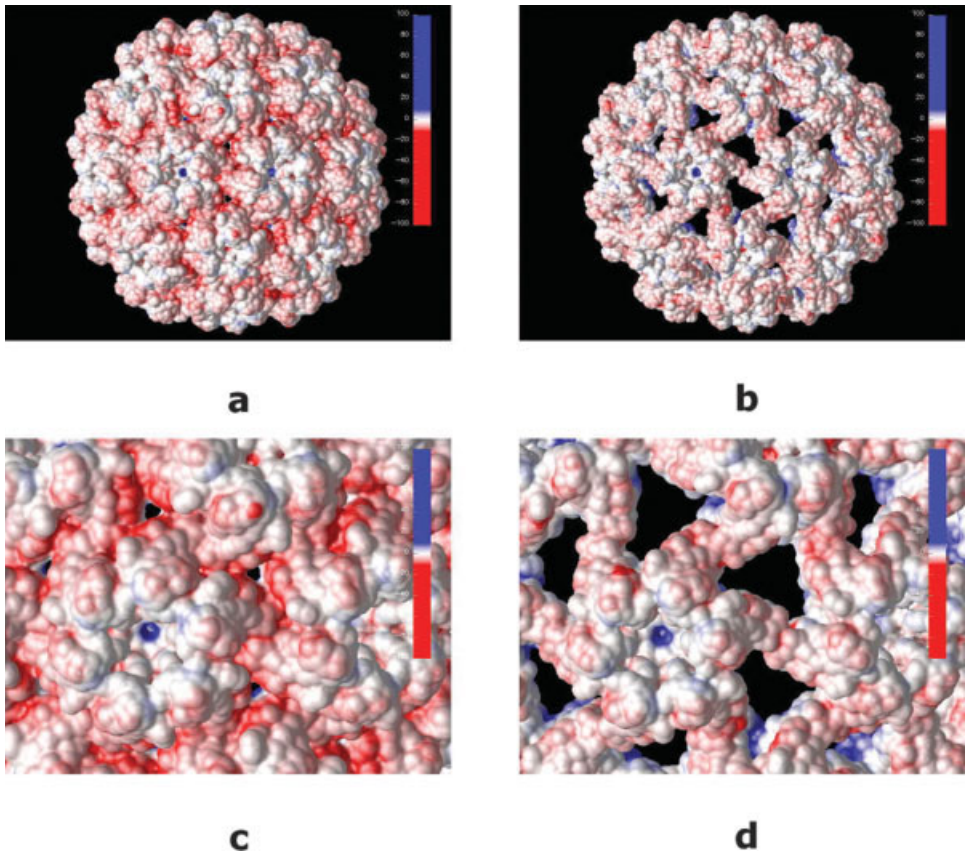

FIGURE 4 Calculated electrostatic potential projected on the solvent accessible surface of the native (a and c) and swollen (b and d) CCMV capsid. Subfigures c and d show closeups of the outer capsid shell. Blue and red colors represent positive and negative electrostatic potential, respectively. Hue intensity depicts strength of the potential (in kT/e units) as shown on the scale in the top right corner of each picture.

amino acids in the N-terminal arm (Figure 6). The electrostatic potential on the inner capsid surface is still mostly positive but it is significantly weaker compared to the native structure. This indicates that the capsid shell with the first 26 N-terminal residues deleted can still favorably interact with negatively charged RNA, but the interaction is not strong enough for in vitro assembly of RNA-containing particle.[3]

As the capsid swells, it is interesting to note that surface areas of negative electrostatic potential on the outer capsid shell are exposed (Figure 4b and d). These areas are located at the capsid shell openings created by the capsid expansion. Similarly, the inner swollen capsid surface exposes patches of negative electrostatic potential (Figure 5b and d). This may aid in releasing the enveloped genetic material since the exposed inner surface patches of negative potential will most likely decrease electrostatic binding energy to the negatively charged RNA inside of the capsid. However, since these exposed patches are located at the capsid shell openings at the pseudo-threefold axis they will likely hinder spontaneous RNA release through this openings. We also note that counterion adsorption may stabilize this RNA/capsid protein interaction somewhat.

Cucumber Mosaic Virus (CMV)

The calculated electrostatic potential (visualized as an isosurface at ± 1.0 kT/e) for the CMV capsid is shown in Figure 7. Although CCMV and CMV are structurally remarkably homologous, CMV has only a 19% capsid protein sequence identity (34% similarity) to CCMV.[2] This is reflected in a marked difference between their electrostatic properties. The electrostatic potential at the CMV outer capsid surface is far more neutral, with a similar distribution of negative and positive potential on the surface (Figure 7). While the potential at the pentameric and hexameric subunits is negative, the rest of the capsid surface has a positive electrostatic potential. The negative potential at the hexameric and pentameric subunits is

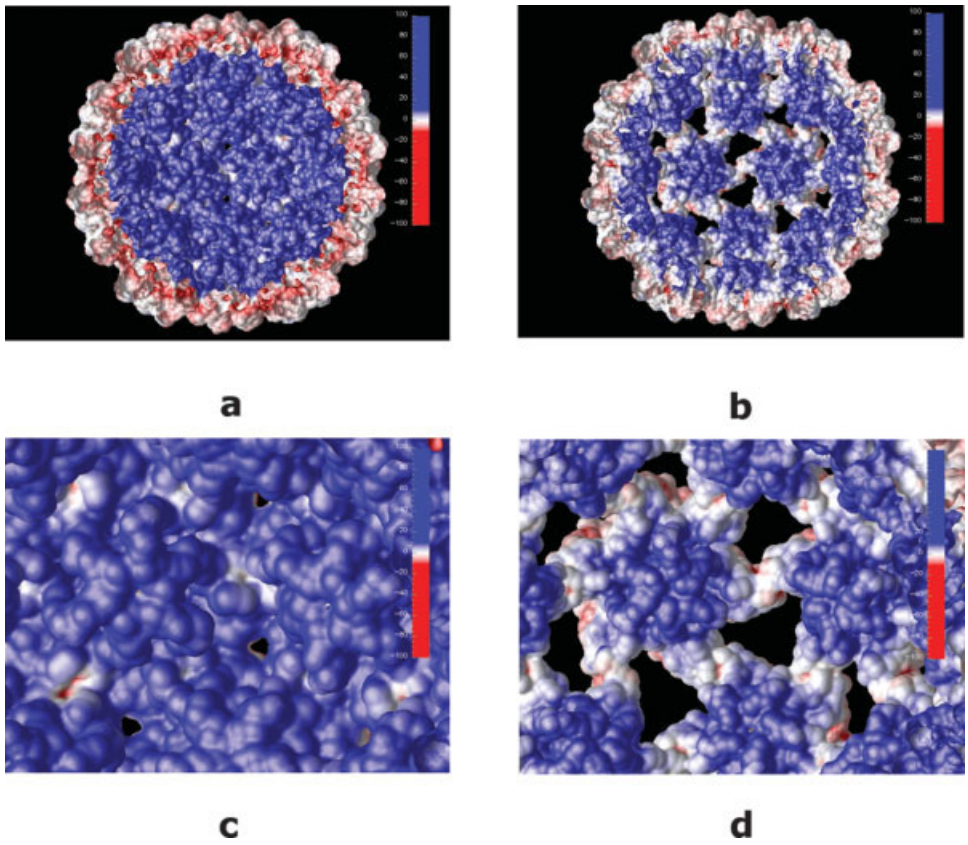

FIGURE 5 Electrostatic potential projected on the solvent accessible surface of the CCMV particle, inner shell surface view. Both the native (a and c) and swollen (b and d) structures are shown. Panels c and d show closeup views of the inner shell.

mainly due to charged amino acid residues in the βH–βI surface loop, which has been shown to play an important role in the CMV virion transmission.[43]

This βH–βI loop has a high degree of amino acid conservation among cucumoviruses and has the same length in CCMV but fewer acidic residues (two vs. five). A similar electrostatic potential distribution is observed when the potential is projected on the solvent accessible surface (Figure 8). A closeup of the outer capsid surface (Figure 8b) reveals that there is

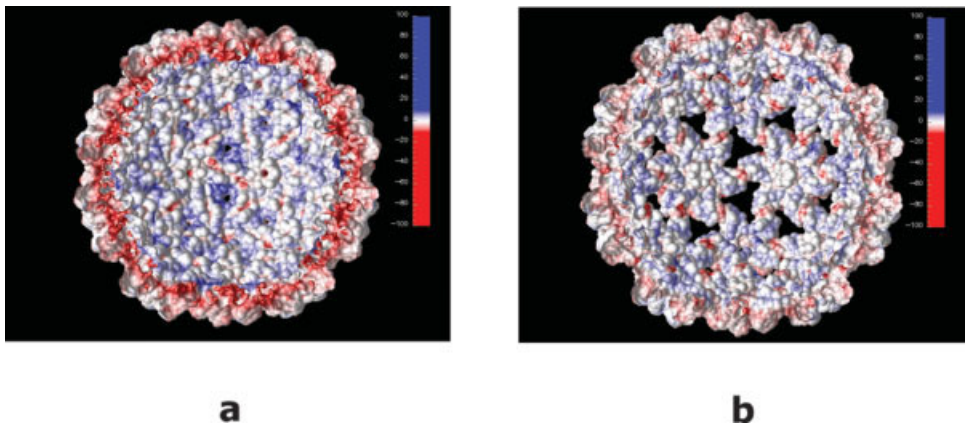

FIGURE 6 Calculated electrostatic potential projected on the solvent accessible surface of the inner shell of the CCMV capsid. The first 26 N-terminal amino acid residues were deleted. Panels a and b show the native and swollen structures, respectively.

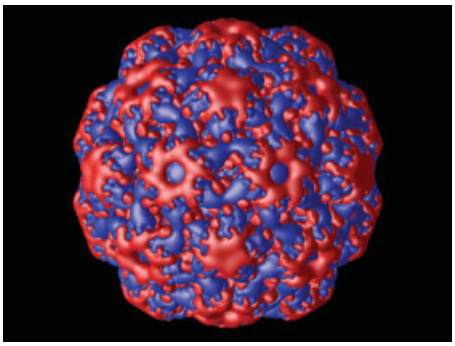

FIGURE 7 Calculated electrostatic potential presented as isosurface (at $\pm 1.0\ kT/e$) of the CMV viral particle. Blue and red colors represent positive and negative potential, respectively.

no high electrostatic potential concentration between the hexameric and pentameric subunits as compared to CCMV. In fact, in CMV the cluster of aspartic residues at the pseudo-threefold axis is replaced by complementing acids and bases, which could explain the insensitivity of the capsid to changes in pH or metal concentration.[9,17]

The relatively weak electrostatic potential on the CMV inner capsid surface (Figure 8c and d), compared to the inner surface potential of the CCMV particle with first 26 N-terminal residues deleted (Figure 6) suggests that CMV without the first 28 N-terminal residues is also not likely to undergo assembly of RNA-containing particles. This prediction is yet to be tested.

Calcium Binding to CCMV

Three binding sites for the calcium ions in one unit of the CCMV virus have been proposed.[1,9] They are situated at the interface of the subunits A–B, B–C, and C–A. The calcium cavity residues are shown in Figure 1c and d. In the native form the cavity is composed of residues Glu81, Lys84, Gln85, Glu148, and Gln149* and Asp153* from the adjacent subunit. Two carbonyl and four carboxyl oxygens contribute to bonding of the Ca^{2+} ion. Binding energies from gas-phase equilibria confirm that there is preference of Ca^{2+} for six-ligand interactions.[44] After the swelling, Gln149* and Asp153*, which lie at the border

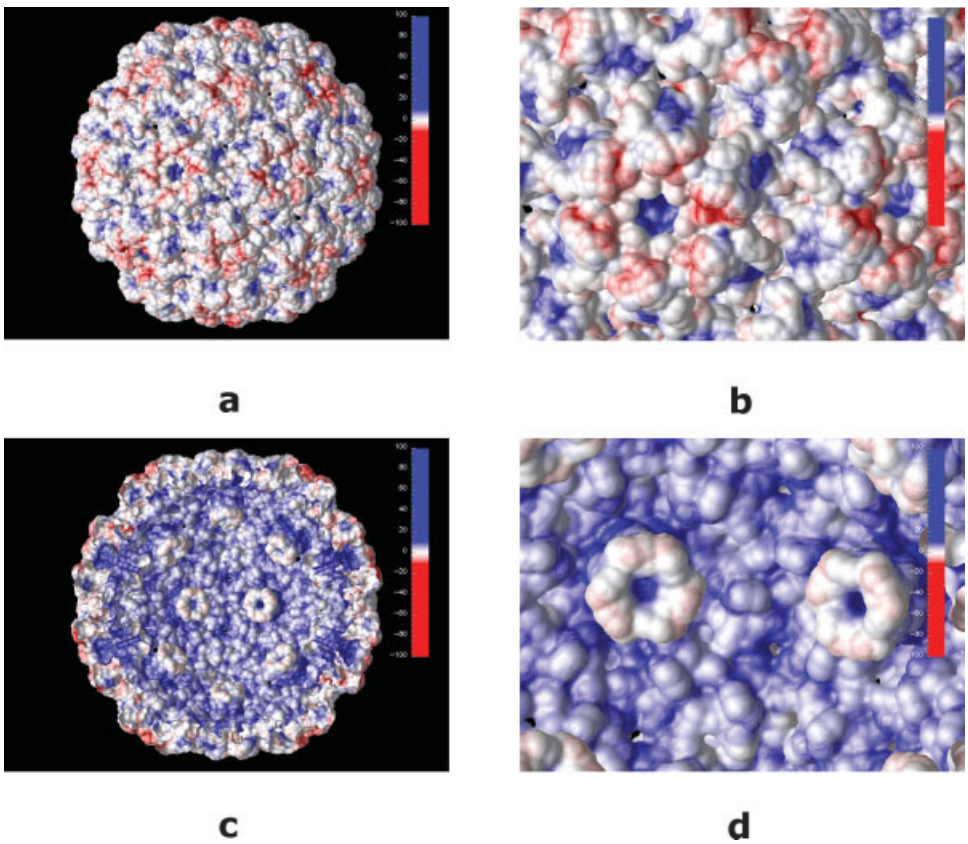

FIGURE 8 CMV calculated electrostatic potential projected on the solvent accessible surface. Both outer (a and b) and inner (c and d) surface of the capsid shell are shown. Subfigures b and d show a magnified view of the shell surface.

Table I Electrostatic Contribution to Ca^{2+} Binding Free Energy for Fragments of the CCMV Virion (kcal/mol)[a]

	One Calcium Cavity		One Protein Unit	
Force Field	$\Delta G_{elec}^{solv+coul}$	$\Delta G_{elec}^{directly}$	$\Delta G_{elec}^{solv+coul}$	$\Delta G_{elec}^{directly}$
Linear PBE				
charmm19	−58.7	−57.7	−79.6	−78.6
charmm22	−39.1	−38.6	−70.5	−69.3
charmm22/ESP	−43.2	−43.1	−67.9	−66.9
Nonlinear PBE				
charmm19	−58.9	−57.3	−74.8	−73.6
charmm22	−39.3	−38.9	−65.0	−64.8
charmm22/ESP	−43.3	−43.3	−64.3	−64.1

[a] Results obtained directly and by splitting into solvation and coulombic contributions are compared. The energy terms are shown per one calcium, and for one cavity were averaged over cavities A, B, and C; for one protein unit were averaged over three Ca^{2+}.

between subunits, escape from the cavity and the number of coordinating bonds is reduced to five. Consequently, calcium binding is weakened, yet electrostatic interactions are still favorable. The tendency to form a six-coordinated calcium might be another reason for conformational change from the swollen to the native state. The affinity for the calcium in the cavity must be high enough to prevent its escape into the surrounding aqueous solution. The net charge of the residues within 20 Å from the calcium ion changes from $-5e$ in the native form to $0e$ in the swollen form, indicating that the environment in the swollen form is less electrostatically favorable to bind calcium.

The electrostatic binding energies for one calcium cavity and one native protein unit, comparing the direct and additive calculation method, and the linear and nonlinear solution to the PB equation, are presented in Table I. Overall, as expected, the electrostatic term is largely favorable.[45] The ΔG_{elec} was calculated assuming an uniform dielectric constant of the protein (ε) equal to 2. For a twice as high dielectric of 4, ΔG_{elec} for a Na^+ ion binding to an acidic residue but on the protein surface was calculated as −10 kcal/mol.[46] In the CCMV case, the electrostatic contribution is expected to be much larger since a doubly charged ion interacts with at least five oxygens and a smaller dielectric constant was used in our calculation. The energetics of charge–charge interactions for Ca^{2+} binding to solvent-exposed acidic residues in α-lactalbumin[47] calculated with a PB equation and a single-site model with $\varepsilon = 20$[48] predicted energy of −20 kcal/mol. Again, we use a 10-fold lower ε with a more detailed charge model and the cavity residues are not exposed to solvent, so we expect our values to be larger.

The electrostatic contribution to binding calculated for one cavity is less negative than the average electrostatic binding energy of one calcium in one protein unit. This suggests that the local environment is not the only contribution to the binding. Indeed, the net charge of the cavity without calcium is $-2e$ and within 20 Å of the ion it is $-5e$, suggesting that the binding might be more favorable to the whole unit. The differences between the ΔG_{elec} calculated with the direct and additive approach for one cavity and for one protein unit are less than 1 kcal/mol. The additive method requires twice as many PB calculations and additionally the calculation of the coulombic term. This method should be, in principle, more accurate because it does not depend on the placing of molecules on the grid. The direct method needs only three calculations, but with the same placing on the grid of both the complex, and the ligand and the protein, separately. The agreement of the two methods is very good, indicating that for this grid resolution one may use the simpler and faster approach. For one cavity, the energies determined with the linear solution to the PBE are in excellent agreement. For one unit the values cannot be compared because different convergence was obtained with the linear and nonlinear solutions to the PBE (see Materials and Methods).

In the case of one protein unit, we investigated if there is any cooperativity in the electrostatic contribution for the calcium binding. We compared the ΔG_{elec} of the binding of one calcium alone with the binding of the same calcium if another one was already present in the system. Calcium ions are

Table II Electrostatic Contribution to Ca^{2+} Binding Energy for the Whole CCMV Virion (kcal/mol) Obtained Directly and by Splitting into Solvation and Coulombic Contributions[a]

	Native Form		Swollen Form	
Force Field	$\Delta G_{elec}^{solv+coul}$	$\Delta G_{elec}^{directly}$	$\Delta G_{elec}^{solv+coul}$	$\Delta G_{elec}^{directly}$
Linear PBE				
charmm19	−78.4	−77.9	−8.6	−7.9
charmm22	−73.4	−69.1	−21.7	−21.0
charmm22/ESP	−70.3	−66.9	−20.3	−19.8
Nonlinear PBE				
charmm19	−78.9	−78.4	−8.8	−8.1
charmm22	−71.9	−67.6	−22.7	−22.0
charmm22/ESP	−70.0	−66.4	−21.0	−20.6

[a] The energy terms are per one calcium ion and were calculated for the whole native and swollen CCMV virus with different force field parameters and averaged over 180 ions.

between 11 and 13 Å apart in the native form. It turns out that the difference in ΔG_{elec} is less than 3 kcal/mol; therefore, cooperativity is not detected with the PB approach. On the other hand, we do not have evidence that it exists for this system.

Table II shows the electrostatic contributions to calcium-binding energies for the whole native and swollen CCMV capsid. The relative calcium electrostatic binding energies are substantial; the electrostatic contribution to the native form of the virus is at least three times more favorable, depending on the force field parameters used. If one compares the appropriate energy values of Tables I and II for the native form of the virus, one may notice that for all the force fields ΔG_{elec} calculated with the nonlinear PB equation is more favorable for the whole CCMV in comparison to the value determined for one protein unit, but the differences do not exceed 10%. This suggests that the one protein unit environment provides most of the favorable electrostatic contribution for calcium binding. This observation is in accord with the study of energetics of charge–charge interactions in α-lactalbumin upon Ca^{2+} binding.[47] It was shown that calcium binding only slightly affects the distant residues and does not change their charge–charge interactions.

The electrostatic contribution to binding energies of calcium to the swollen form is reduced but is still negative even with the united atom model force field of charmm19 (Table II). This is expected because the surrounding overall charge (within 20 Å of calcium ion) is not as negative as in the native form. Additionally, in the native form the calcium ion is coordinated by six oxygens and in the swollen form only by five.

We have also attempted to estimate the calcium ion relative binding free energies in the native and swollen CCMV forms by estimating the ΔG_{np} and $-T\Delta S$ terms. The volume of the Ca^{2+} is very small in comparison to the volume of ligands usually binding to proteins and calcium ion is bound in a tight cavity and is inaccessible to solvent. The difference in the solvent accessible area upon binding of one Ca^{2+} to the CCMV binding cavity is 129 $Å^2$, which is the SASA of the free Ca^{2+}. This SASA difference is similar in the native and swollen forms of the virus. Estimating an upper limit of ΔG_{np} by multiplying the change in SASA by one of the highest proportionality constants applied in literature (60 cal/mol $Å^2$)[27,49] gives a value for ΔG_{np} less than 2 kcal/mol, which is negligible in comparison to the electrostatic contribution. Additionally, the nonpolar term is presumably similar in the native and swollen forms and cancels out.

For similar reasons, the difference in entropy loss $-T\Delta S$ should be approximately equal in both forms of CCMV, and significantly smaller than the difference in ΔG_{elec}. Based on a rigid structure it is impossible to correctly calculate the $-T\Delta S$ term of calcium and cavity residues upon binding, but one may estimate this quantity based on literature and calculations for other systems.

We do not know how flexible the residues are without the presence of calcium. One of the glutamates, Glu81, may be protonated without Ca^{2+} and stabilize the cavity residues[9]; the presence of water molecules may not be excluded. To estimate how Ca^{2+} shields the cavity residues from water, we calculated the difference in SASA between the native structure with and without the calcium ion. This difference equals 111 $Å^2$ and if we assume that the whole value comes from the six cavity residues it is 18.5 $Å^2$ per residue. This number is small and shows

that Ca^{2+} changes the solvent exposure of the cavity residues only negligibly. Moreover, this change originates only from side chains; main chains are shielded even prior Ca^{2+} binding, so we do not account for their entropy change. If we assume that the side chains are ''free'' before and completely ''restricted'' to one rotamer upon calcium binding, we can estimate an upper limit of entropy loss for the cavity residues. The work of Pickett and Sternberg[50,51] predicted an empirical scale of entropy loss per side chain upon folding depending on the residue type. Following this scale, the loss for the native cavity would be at most 11 kcal/mol and for the swollen 7.6 kcal/mol. Based on the fluctuations in molecular dynamics simulations, Friedman et al.[46] estimated that Cl^- binding to a residue on the protein surface does not affect the fluctuations of that residue. Therefore, we assume that the translational and rotational entropy loss for the cavity residues is not influenced by the binding of an ion.

Translational entropy loss of calcium ion upon binding is also difficult to estimate. It was shown that Ca^{2+} forms stable clusters with up to eight water molecules.[45] Therefore, its motion is already heavily constrained prior binding by interactions with aqueous environment. The interactions in the cavity stabilize calcium as well to override favorable interactions in water. The calculated entropy loss for ligands is typically between 4 and 7 kcal/mol (see Refs. 52 and 53, and references therein). We suppose that calcium is probably more restricted and detained in the cavity than an uncharged ligand binding to protein, and the upper limit of the difference between translational entropy in water and in cavity may be closer to the higher value. Comparably, Friedman et al.[46] predicted the translational $T\Delta S$ of the Na^+ ion as -2.5 kcal/mol. Considering the above, an upper estimate of the overall $-T\Delta S$ term for the swollen form should not exceed 14 kcal/mol. Even without including the small (less than 2 kcal/mol) but favorable nonpolar contribution, calcium shows favorable binding in the expanded form for charmm22 and charmm22/ESP force fields. In charmm19 there would be no binding, but it is an united atom model and it might not work well with such a complex problem as binding of metal to a protein and may be too crude an approximation. With an all-atom parameter set, calcium is predicted to be capable of binding to the swollen form of CCMV, which suggests that it facilitates the stabilization of the native form, and most probably induces the viral contraction. With a high concentration of Ca^{2+}, the CCMV viral capsid may not swell because its native form is highly stabilized.

Concluding, the binding energy estimate shows that calcium affects the structural flexibility of the virion and that the electrostatic contribution is still favorable even when the virus is in its expanded form.

However, the calculation results depend upon the parameters used in the PB equation, but we were primarily interested in the differences of calcium affinity to the native and swollen states and not in the absolute binding energy values. We tested a few sets of charges and radii and two approaches for calculating the binding energies, direct and by splitting into coulombic and desolvation contributions; both methods gave comparable results. The main drawback of this kind of binding energy calculation is the single-conformation approximation and assumption of an uniform dielectric constant of the protein, but nevertheless on average we see noticeable differences in the binding of calcium to the native and swollen forms of CCMV.

CONCLUSIONS

Assembly and disassembly and RNA release mechanisms of the cowpea chlorotic mottle viral capsid are still poorly understood, despite the capsid's relative simplicity and available detailed experimental information. We have examined the role electrostatics plays in these processes. The calculated electrostatic potentials for the native and swollen CCMV structures confirm that electrostatic repulsion at the pseudo-threefold axis sites is most likely the driving force for the capsid swelling. Strong positive electrostatic potential on the inside, inner capsid shell suggests that electrostatic interactions between enveloped, negatively charged RNA and the inner capsid shell are dominant. As the capsid swells, patches of negative electrostatic potential on the capsid surface are exposed, which destabilizes RNA–capsid interaction and may aid in the RNA release process. It is unlikely that the RNA could escape from the inside of the capsid (at neutral pH) through chanels formed by the swelling due to electrostatic repulsion.

Cucumber mosaic virus, which is highly homologous to CCMV, has complementary distribution of negative and positive electrostatic potential at the pseudo-threefold axis sites, rendering the virion incapable of swelling.

The electrostatic contributions to binding free energy of site-bound Ca^{2+} to the whole CCMV were estimated by means of the continuum solvent PB approach. The size of the grid in the extremely large calculations exceeded $500 \times 500 \times 500$ Å^3, but we were able to reach a grid resolution of 0.4 Å (more

than 2.5 billion grid points). The calculations show the differences in the electrostatic binding energies between the swollen and native CCMV forms, from 46 to 70 kcal/mol, depending on the force field parameters. The average electrostatic contribution in the native form is fairly large, but the native form is already the most stable one; therefore, estimated binding energies to the native state are exaggerated. On the other hand, the calcium-binding energies must be substantial relative to that with water to provide stability of the ion in protein relative to that in aqueous solution. Our calculations are restricted to two rigid conformations, with the swollen state being a model, so only the qualitative picture and relative energies with respect to the native state are available. Additionally, the electrostatic contribution depends strongly on the used dielectric constant of the protein capsid in the PB calculation (see, e.g., Ref. 46).

Since binding of calcium is reversible, ions most probably start binding to the more expanded form and induce viral contraction. CCMV expansion takes away two cavity residues from the adjacent subunit and the number of coordinating oxygens is reduced from six to five, yet electrostatic contribution to calcium binding is still favorable. By estimating an upper limit of the nonpolar and entropic contributions, we see overall favorable calcium binding even in the swollen state. Small but favorable binding affinity to the expanded state may help in stabilizing the virus in its native form.

The average electrostatic energies for one calcium ion binding to one protein unit and for the whole CCMV structure differ by less than 10%. However, the electrostatic binding energy to one calcium cavity is less negative, implicating the importance of the surrounding on binding. The linear and nonlinear PB equation give comparable values. The direct and additive method of calculating the binding energy gave similar results, suggesting that the effect of placing molecules on the grid does not contribute much in case of our system.

In addition to the conclusions presented above, this work demonstrates that more detailed calculations are feasible on this system and, in future work, can be used to interpret local changes on the atomic scale (e.g., point mutants, detailed pKa calculations, etc.).

We are very grateful to Wayne Pfeiffer, Giri Chukkapalli, and the San Diego Supercomputer Center for providing access to Blue Horizon and Data Star supercomputers and for their generous technical assistance. We would also like to thank the W. M. Keck Foundation and the NSF Center for Theoretical Biological Physics (CTBP) for providing additional computational resources. This work was supported in part by NIH, NSF, the National Biomedical Computing Resource, CTBP, and Accelrys, Inc. NAB was supported by a Research Fellowship from the Alfred P. Sloan Foundation and grant GM069702 from the NIH. CLB and FT acknowledge the support of the NSF (CTBP) and NIH through the grant RR12255 (MMTSB). JT was supported by the Polish Ministry of Science and Information Society Technologies (115/E-343/ICM/BST-1076/2005) and by European CoE MAMBA.

REFERENCES

1. Speir, J. A.; Munshi, S.; Wang, G. J.; Baker, T. S.; Johnson, J. E. Structure 1995, 3, 63–78.
2. Smith, T. J.; Chase, E.; Schmidt, T.; Perry, K. L. J Virol 2000, 74, 7578–7586.
3. Zhao, X.; Fox, J. M.; Olson, N. H.; Baker, T. S.; Young, M. J. Virology 1995, 207, 486–494.
4. Fox, J. M.; Zhao, X.; Speir, J. A.; Young, M. J. Virology 1996, 222, 115–122.
5. Fox, J. M.; Albert, F. G.; Speir, J. A.; Young, M. J. Virology 1997, 227, 229–233.
6. Albert, F. G.; Fox, J. M.; Young, M. J. J Virol 1997, 71, 4296–4299.
7. Bancroft, J. B. Adv Virus Res 1970, 16, 99–134.
8. Jacrot, B. Mol Biol 1975, 95, 433–446.
9. Tama, F.; Brooks, C. L., III. J Mol Biol 2002, 318, 733–747.
10. Liu, H.; Qu, C.; Johnson, J. E.; Case, D. A. J Struct Biol 2003, 142, 356–363.
11. Zlotnick, A.; Aldrich, R.; Johnson, J. M.; Ceres, P.; Young, M. J. Virology 2000, 277, 450–456.
12. Zhang, D.; Konecny, R.; Baker, N. A.; McCammon, J. A. Biopolymers 2004, 75, 325–337.
13. Isea, R.; Aponte, C.; Cipriani, R. Biophys Chem 2004, 107, 101–106.
14. Witz, J.; Brown, F. Arch Virol 2001, 146, 2263–2274.
15. Allouche, D.; Parello, J.; Sanejouand, Y.-H. J Mol Biol 1999, 285, 857–873.
16. Li, P. P.; Naknanishi, A.; Tran, M. A.; Ishizu, K. I.; Kawano, M.; Phillips, M.; Handa, H.; Liddington, R. C.; Kasamatsu, H. J Virol 2003, 77, 7527–7538.
17. Wikoff, W. R.; Tsai, C. J.; Wang, G.; Baker, T. S.; Johnson, J. E. Virology 1997, 232, 91–97.
18. Garrett, A. J. M.; Poladian, L. Ann Phys 1988, 188, 386–435.
19. Sharp, K. A.; Honig, B. Ann Rev Biophys Chem 1990, 19, 301–332.
20. Baker, N. A.; McCammon, J. A. Electrostatic Interactions. In Structural Bioinformatics; Weissig, H., Bourne, P. E., Eds.; John Wiley & Sons: New York, 2003, pp 427–440.
21. Tirion, M. M. Phys Rev Lett 1996, 77, 1905–1908.
22. Bahar, I.; Atilgan, A. R.; Erman, B. Fold Des 1997, 2, 173–181.
23. Tama, F.; Sanejouand, Y. H. Protein Eng 2001, 14, 1–6.

24. Tama, F.; Wriggers, W.; Brooks, C. L., III. J Mol Biol 2002, 321, 297–305.
25. Tama, F.; Gadea, F. X.; Marques, O.; Sanejouand, Y. H. Proteins 2000, 41, 1–7.
26. Tama, F.; Brooks, C. L., III. In Normal Mode Analysis: Theory and Applications to Biological and Chemical Systems; Cui, Q., Bahar, I., Eds.; CRC Press: Boca Raton, FL, 2005.
27. Froloff, N.; Windemuth, A.; Honig, B. Protein Sci 1997, 6, 1293–1301.
28. Lazaridis, T. Curr Org Chem 2002, 6, 1319–1332.
29. Gilson, M. K.; Sharp, K. A.; Honig, B. H. J Comput Chem 1988, 9, 327–335.
30. Misra, V. K.; Draper, D. E. J Mol Biol 1999, 294, 1135–1147.
31. Misra, V. K.; Draper, D. E. J Mol Biol 2000, 299, 813–825.
32. Misra, V. K.; Draper, D. E. Proc Natl Acad Sci USA 2001, 98, 12456–12461.
33. Baker, N. A.; Sept, D.; Joseph, S.; Holst, M. J.; McCammon, J. A. Proc Natl Acad USA 2001, 98, 10037–10041.
34. Berman, H. M.; Westbrook, J.; Feng, Z.; Gilliland, G.; Bhat, T. N.; Weissig, H.; Shindyalov, I. N.; Bourne, P. E. Nucleic Acids Res 2000, 28, 235–242.
35. Trylska, J.; Konecny, R.; Tama, F.; Brooks, C. L., III. McCammon, J. A. Biopolymers 2004, 74, 423–431.
36. Yang, A. S.; Gunner, M. R.; Sampogna, R.; Sharp, K.; Honig, B. Proteins Struct Funct Genet 1993, 15, 252–265.
37. Brooks, B. R.; Bruccoleri, R. E.; Olafson, B. D.; States, D. J.; Swaminathan, S.; Karplus, M. J Comp Chem 1983, 4, 187–217.
38. MacKerell, A. D., Jr.; Brooks, B.; Brooks, C. L., III; Nilsson, L.; Roux, B.; Won, Y.; Karplus, M. In The Encyclopedia of Computational Chemistry, Vol. 1; v. R. Schleyer et al., P., Ed.; John Wiley & Sons: Chichester, 1998, pp 271–277.
39. Frisch, M. J.; et al. Gaussian 98, Revision A.11.4; Gaussian, Inc.: Pittsburgh, PA, 2002.
40. Becke, A. D. J Chem Phys 1993, 98, 5648–5652.
41. Lee, C.; Yang, W.; Parr, R. G. Phys Rev B 1988, 37, 785–789.
42. Chirlian, L. E.; Franc, M. M. J Comp Chem 1987, 8, 894–905.
43. Liu, S.; He, X.; Park, G.; Josefsson, C.; Perry, K. L. J Virol 2002, 76, 9756–9762.
44. Peschke, M.; Blades, A. T.; Kebarle, P. J Am Chem Soc 2000, 122, 10440–10449.
45. Pavlov, M.; Siegbahn, P. E. M.; Sandstrom, M. J Phys Chem A 1998, 102, 219–228.
46. Friedman, R.; Nachliel, E.; Gutman, M. Biophys J 2005, 89, 768–781.
47. Permyakov, S. E.; Makhatadze, G. I.; Owenius, R.; Uversky, V. N.; Brooks, C. L.; Permyakov, E. A.; Berliner, L. J. Protein Eng Des and Sel 2005, 18, 425–433.
48. Antosiewicz, J.; McCammon, J. A.; Gilson, M. K. J Mol Biol 1994, 238, 415–436.
49. Nicholls, A.; Sharp, K. A.; Honig, B. Proteins 1991, 11, 281–296.
50. Pickett, S. D.; Sternberg, M. J. E. J Mol Biol 1993, 231, 825–839.
51. Doig, A. J.; Sternberg, M. J. E. Protein Sci 1995, 4, 2247–2251.
52. Lazaridis, T.; Masunov, A.; Gandolfo, F. Proteins 2002, 47, 194–208.
53. Swanson, J. M. J.; Henchman, R. H.; McCammon, J. A. Biophys J 2004, 86, 67–74.
54. Reddy, V. S.; Natarajan, P.; Okerberg, B.; Li, K.; Damodaran, K. V.; Morton, R. T.; Brooks, C. L., III; Johnson, J. E. J Virol 2001, 75, 11943–11947.

Reviewing Editor: David Case